Analysis and Design of the Dickson Charge Pump for sub-50 mV Energy Harvesting

Marcio Bender Machado[a], Franciele Nornberg[b,*], Mohamad Sawan[c,d], Carlos Galup-Montoro[b], Marcio Cherem Schneider[b]

[a] *Federal Institute of São Paulo, Brazil*
[b] *Federal University of Santa Catarina, Brazil*
[c] *École Polytechnique de Montréal, Canada*
[d] *School of Engineering, Westlake University, Hangzhou, China*

Abstract

This paper presents the analysis and design of a DC/DC boost converter operating from supply voltages around the thermal voltage (26 mV at room temperature), for energy harvesting applications. The boost converter described herein is aimed at starting up DC/DC converters, but its use can be extended to a conventional DC/DC converter in which the power conversion efficiency is not of major concern. Firstly, the operation of the Dickson charge pump for ultra-low voltage is described. Expressions for the output voltage, power conversion efficiency and input resistance are derived. The extremely low voltage operation, made feasible through an enhanced-swing ring oscillator and zero-VT transistors, is demonstrated via a prototype fabricated in 130 nm CMOS technology. For an input voltage of 17 mV, the converter delivers an output current of 10 nA at 1 V output and provides a current of 1 μA at a DC output of 1 V from an input voltage of 23 mV.

Keywords:
Dickson charge pump, ultra-low voltage, ultra-low power, energy harvesting, zero-VT MOSFET

*Corresponding author.
Email address: francielefnornberg@gmail.com (Franciele Nornberg)

1. Introduction

Charge pump converters introduced by Dickson [1] have been employed in a wide variety of applications, including bias generators for dynamic random access memory and flash memory, drivers for light emitting diodes and liquid crystal displays, and AC-DC converters that harvest energy from an RF signal [2]. In the energy scavenging field, the demand for energy autonomy has driven the search for boost converters able to operate from extremely low voltages. *In vivo* monitoring of the activity of human organs (*e.g.* through electrocardiograms, electroencephalograms, or intraocular pressure examinations) and the stimulation of human tissue, which generally consume some dozens of micro-watts [3, 4], could lead to a new class of ultra-low-power (ULP) and ultra-low-voltage (ULV) energy harvesters.

Solar cells in dark environments [5], wearable thermoelectric generators [6, 7, 8] and implantable glucose fuel cells [9], which typically generate less than 100 mV, are appealing choices to power the electronics of sensor networks and biomedical appliances. However, given the ULV levels generated by these energy harvesters, a boost converter is required to power conventional electronics which, in general, needs supply voltages of around 1 V. In the past decade, in an attempt to reduce the minimum voltage required to start up converters, many researchers have presented solutions employing schematics based on charge pumps or inductive boost converters. A challenge in the design of converters powered from voltages below 50 mV is the start-up stage, due to the low efficiency of devices operating at ULV and the need to generate oscillatory signals from such a low voltage.

In [3], a body sensor node is powered from a supply voltage of 30 mV of a thermoelectric harvester, but wireless RF power is provided for the kick start. In [10], a boost converter that uses off-chip inductors starts up at a minimum voltage of 50 mV . In [11], a 35 mV boost converter is presented; however, it requires a mechanical switch for the kick start of the converter. A start-up converter of 80 mV is presented in [12], but it requires a threshold-voltage-tuned oscillator in order to decrease the minimum start-up voltage. In recent publications [13, 14, 15], fully integrated solutions with no tuning processes are proposed, but they operate from around 100 mV .

In order to deal with the conflicting requirements of very low voltage for the converter start-up and the high power conversion efficiency, the use of a hybrid configuration composed of two converters, similar to that shown in Fig. 1, has been widely employed [6, 7, 14, 16, 17, 18, 19]. Reference [6]

reports a thermoelectric energy harvester which starts up from 65 mV. In [7], an on-chip transformer-based LC oscillator starts up at an open-circuit-voltage of 160 mV . [14] presents a converter which starts up from 100 mV. [16] reports a DC-DC converter that operates from a 7 mV supply voltage, but requires a minimum self-start voltage of 210 mV . In [17], a start-up converter based on a ring oscillator and a charge pump starts up at 60 mV. In the converter of [18], an inductor of the start-up Colpitts oscillator is reused in the main boost converter to minimize the number of off-chip components, but it starts up from a minimum of 40 mV.

In general, the start-up converter, responsible for the initial operation of the harvester, is composed of an oscillator and a charge pump. The main requirement for this block is to start up from a very low voltage, *i. e.* 50 mV or even less. Power conversion efficiency is not the primary concern for the start-up block, since it can be turned off after the voltage on capacitor C has reached the minimum voltage required to operate the high-efficiency converter. To kick start the circuit at extremely low voltages, a charge pump has been commonly used.

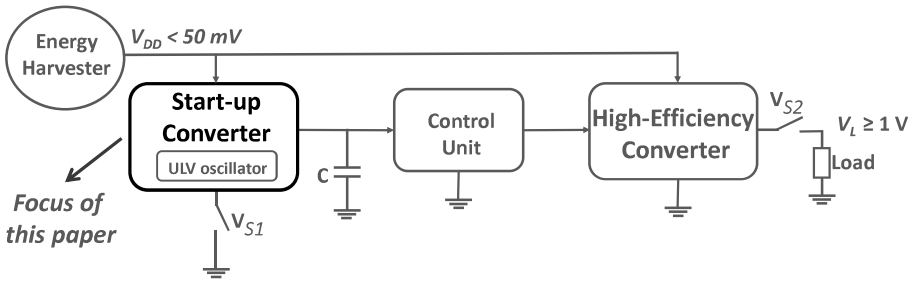

Figure 1: Hybrid configuration composed of two voltage converters.

Aiming at the generation of a DC voltage to kick-start boost converters or directly supply micro-watt loads from extremely low voltages, this paper presents an analysis of the Dickson charge pump (DCP), which includes the forward voltage drop across the diodes in terms of the diode parameters, the number of stages, and the load current. Expressions for the output voltage, power efficiency and input resistance, valid for ULV operation, are derived. Using an enhanced swing ring oscillator, together with a DCP, we designed and tested a prototype built with zero-VT transistors and high quality factor inductors, aimed at converting DC input voltages of the order of 20 mV to 1 V.

The paper is organized as follows. Section 2 presents the ULV model of the DCP. The design of the ULV converter prototype is shown in Section 3. Section 4 reports the experimental results for the converter prototype. Section 5 details the conclusion based on the findings reported in this paper.

2. Analysis of the ULV Dickson charge pump

The analysis of the DCP in reference [1] includes three terms that contribute to the reduction of the output voltage as compared to the ideal case. These terms are the attenuation of the clock voltage due to the stray capacitances, the voltage ripple on the capacitors, and the forward voltage drop across the diodes. The first two factors are analyzed in [1], but the voltage drop in the diodes, which is the main degradation factor of the performance of the DCP at ultra-low voltages, was not deduced. This paper reviews the analysis of the forward voltage drop across the diodes as a function of the load current and the diode parameters. We have also expanded the model of [13] to include the efficiency as well as the input resistance of the DCP . The analysis herein assumes that all diodes are identical, the ripple voltage is negligible, and the stray capacitances are much smaller than the coupling capacitances. In this work, similarly to the rectifier analysis described in [20], the diode parameters I_S, the saturation current, the ideality factor (n) and the load current (I_L) are included to model the DCP down to ultra-low voltages.

For the N-stage Dickson converter in Fig. 2, one can calculate the steady state DC output voltage with the following simplifying assumptions: (i) $V_{\phi 1} = -V_{\phi 2} = V_A \cos\theta$; (ii) the capacitors are high enough to preclude any significant variation in the voltages across them; and (iii) the diodes are modeled by the Shockley equation, written below.

$$I_D = I_S \left[\exp\left(\frac{V_D}{n\phi_t} \right) - 1 \right] \tag{1}$$

where ϕ_t is the thermal voltage (kT/q) and V_D is the voltage waveform across the diodes.

2.1. Output voltage

For the sake of completeness, we summarize in this subsection and in Appendix A the derivation of the output voltage presented in [13]. The

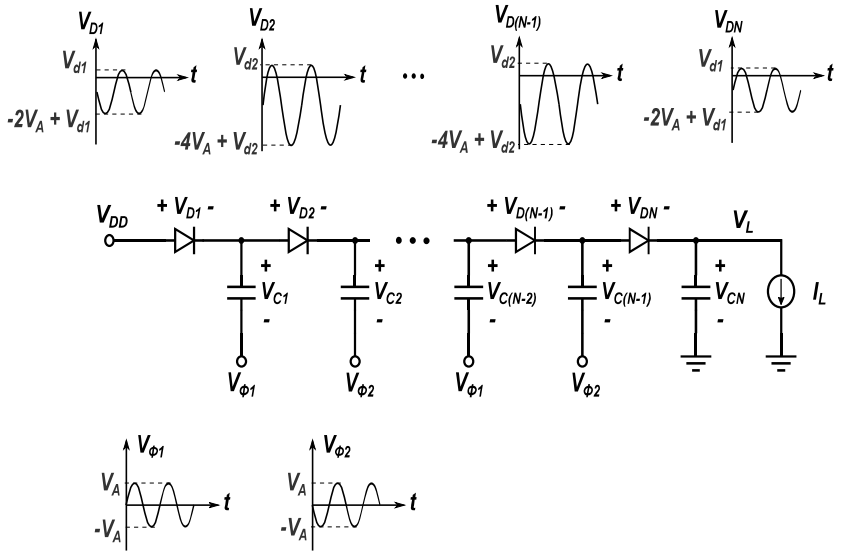

Figure 2: Schematic showing N-stage Dickson charge pump and voltage drop across the diodes.

schematic of the Dickson charge pump, along with the voltage waveforms across the diodes is shown in Fig. 2. The voltage drop across diodes D_1 and D_N differs from that across the other diodes, since one of the terminals of both D_1 and D_N is connected to DC nodes (V_{DD} and V_L, respectively). Noting that $V_{d1} = V_{dN}$, while $V_{d2} = ... = V_{d(N-1)}$, the DC output voltage (V_L) is given by

$$V_L = V_{DD} + (N-1)2V_A - 2V_{d1} - (N-2)V_{d2} \tag{2}$$

Using the diode forward voltage drop derived in Appendix A, the converter output voltage becomes

$$V_L = V_{DD} + 2n\phi_t \ln\left[\frac{I_0\left(v_a\right)}{1 + I_L/I_S}\right] + \left(N-2\right) n\phi_t \ln\left[\frac{I_0\left(2v_a\right)}{1 + I_L/I_S}\right] \tag{3}$$

Here, $v_a = V_A/n\phi_t$ is the normalized magnitude of the oscillator output voltage, and $I_0(z)$ is the modified Bessel function of the first kind of order zero. V_A, the magnitude of the oscillator output voltage, is a function of the DC input voltage and the DCP equivalent input impedance (R_{in}). Simulation of the converter in our design indicated that, for $V_{DD} = 24$ mV and an 11-stage DCP, the value of the oscillator amplitude V_A is less than 100 mV and the output voltage is 1 V for a load of 1 μA.

Expression (3), which is graphically shown in Fig. 3 for the particular case of V_A= 80 mV, is an important tool for the design of charge pumps operating from low voltages. For a given value of v_a one can find a combination of the number of stages and the saturation current that satisfies the design specifications (V_L and I_L).

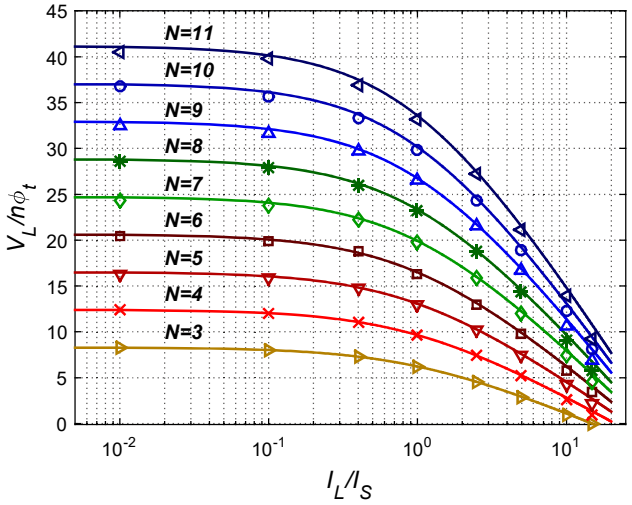

Figure 3: Calculated (solid line) and simulated (symbols) output voltage normalized to thermal voltage ($V_L/n\phi_t$) *vs.* load current normalized to the saturation current (I_L/I_S), for N ranging from 3 to 11, V_{DD} = 30 mV, V_A = 80 mV, and $n\phi_t$ = 27.1 mV.

For $v_a > 3$, $I_0(v_a)$ can be approximated by $exp(v_a)/\sqrt{2\pi v_a}$ with an error below 5 % [21] and Eq. (3) reduces to

$$V_L = V_{DD} + 2(N-1)V_A - Nn\phi_t \ln\left[\sqrt{\frac{2\pi 2V_A}{n\phi_t}}\left(1+\frac{I_L}{I_S}\right)\right] + n\phi_t \ln 2 \quad (4)$$

For the example of Fig. 3, Eq. (4) presents an error of 2 % when compared to Eq. (3), which is affordable considering its simplicity.

2.2. Power conversion efficiency

The power conversion efficiency (PCE) of the DCP is $PCE = P_{out}/P_{in}$, where P_{in} is the output power plus the power dissipated in the diodes.

Using the power loss in the diodes derived in Appendix A yields

$$PCE = \frac{V_{DD} + 2n\phi_t \ln\left[\dfrac{I_0\left(v_a\right)}{1 + I_L/I_S}\right] + \left(N-2\right) n\phi_t \ln\left[\dfrac{I_0\left(2v_a\right)}{1 + I_L/I_S}\right]}{V_{DD} + \left(1 + \dfrac{I_S}{I_L}\right) 2V_A \left[\dfrac{I_1\left(v_a\right)}{I_0\left(v_a\right)} + \left(N-2\right)\dfrac{I_1\left(2v_a\right)}{I_0\left(2v_a\right)}\right]} \tag{5}$$

in which $I_1(z)$ is the modified Bessel function of the first kind of order one.

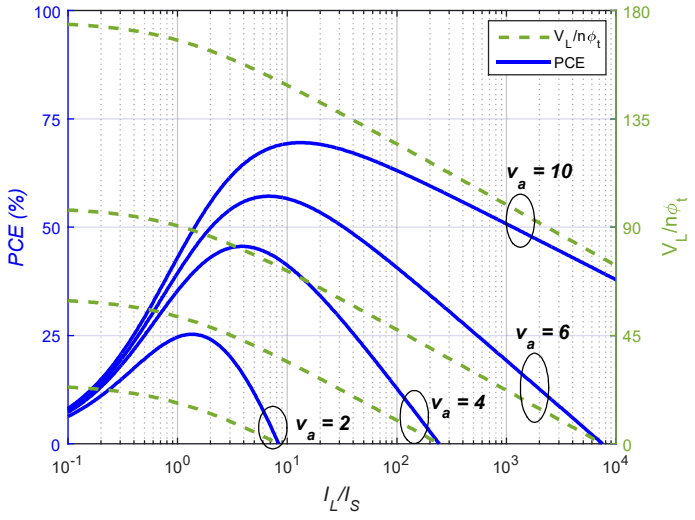

Figure 4: PCE and normalized output voltage of the eleven-stage Dickson converter (for $V_{DD} = 0$) *vs.* normalized load current for normalized peak voltages $v_a = 2$, 4, 6, and 10.

Figure 4 shows the variation of both the output voltage and the PCE of an eleven-stage DCP in terms of I_L/I_S. For a given magnitude applied to the DCP, the PCE reaches, for the case $V_{DD} = 0$, a maximum given [20] by

$$\frac{V_L}{Nn\phi_t} = \frac{I_L}{I_S} \tag{6}$$

Note that, in general, the DC input voltage (V_{DD}) does not have an important contribution to the load voltage, since, usually, $V_{DD} << V_L$.

Equation (3), for the output voltage, and equation (6), for maximizing the PCE are useful for calculating the values of N and I_S for a given V_A at the DCP input.

2.3. Input resistance

Let us now calculate the charge pump input resistance, R_{in}, which loads the oscillator output signals ϕ_1 and ϕ_2. For a sine wave oscillator, the value of $R_{in} = (V_A^2/2)/(P_{in}/2)$ is expressed as

$$R_{in} = \frac{V_A}{2(I_S + I_L)\left[\dfrac{I_1(v_a)}{I_0(v_a)} + (N-2)\dfrac{I_1(2v_a)}{I_0(2v_a)}\right]} \tag{7}$$

in which P_{in} is the total input power delivered by ϕ_1 and ϕ_2 to the charge pump.

When $v_a << 1$, the modified Bessel functions of the first kind reduce to $I_0(v_a) \approx 1$ and $I_1(v_a) \approx v_a/2$ [21]; thus,

$$R_{in,L} = \frac{n\phi_t}{(2N-3)(I_S + I_L)} \tag{8}$$

On the other hand, when $v_a >> 1$, the modified Bessel functions of the first kind are $I_0(v_a) \approx I_1(v_a)$ [21] and the input resistance, becomes

$$R_{in,H} = \frac{v_a n\phi_t}{(2N-2)(I_S + I_L)} \tag{9}$$

Using the results of the prior two equations, the normalized input resistance $r_{in} = R_{in}(I_S + I_L)/n\phi_t$ can be approximated as

$$r_{in} \approx \sqrt{\left(\frac{1}{2N-3}\right)^2 + \left(\frac{v_a}{2N-2}\right)^2} \tag{10}$$

Figure 5 shows the normalized input resistance of the Dickson charge pump versus the number of stages, for $v_a = 2$, 4, and 10. Equation (10) (dashed line) has the benefit of simplicity, at the expense of a maximum error of 6.2 %, as compared to Eq. (7) (continuous line), which uses Bessel functions.

3. Design of the ULV converter

The goal of developing the prototype was to demonstrate the feasibility of the converters operating from very low voltages. The target of the designed

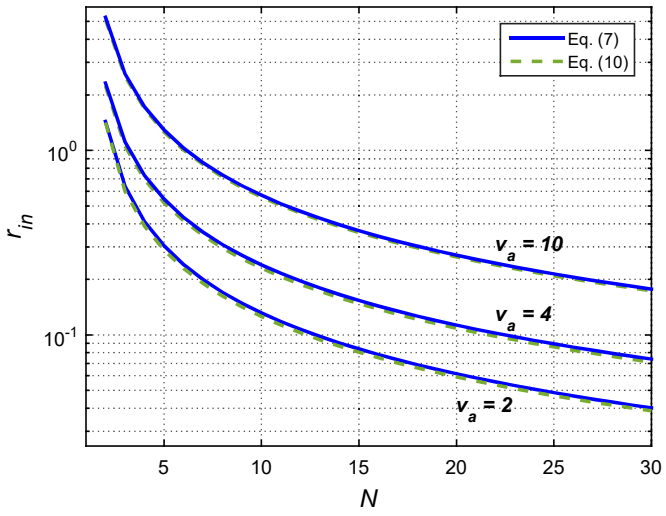

Figure 5: Normalized input resistance of the Dickson converter using Eq. (7) (continuous line) and approximate Eq. (10) (dashed line).

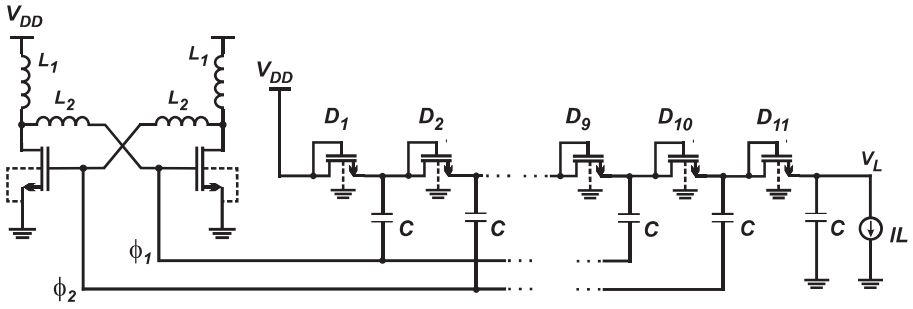

Figure 6: Schematic diagram of the boost converter showing both the ESRO and the DCP.

converter was to give a DC output of 1 V from a DC input voltage of a few tens of mV. The schematic diagram of the converter is shown in Fig. 6.

In order to reduce the prototype area and the losses resulted from the connections between the chip and the external inductors, the chip was wire-bonded to the board substrate using gold wires with a length of 1.5 mm. . Figure 7 shows a photograph of the board employed to test the chip.

Some design details of both the oscillator that generates the complementary signals and the DCP are presented in the following subsections.

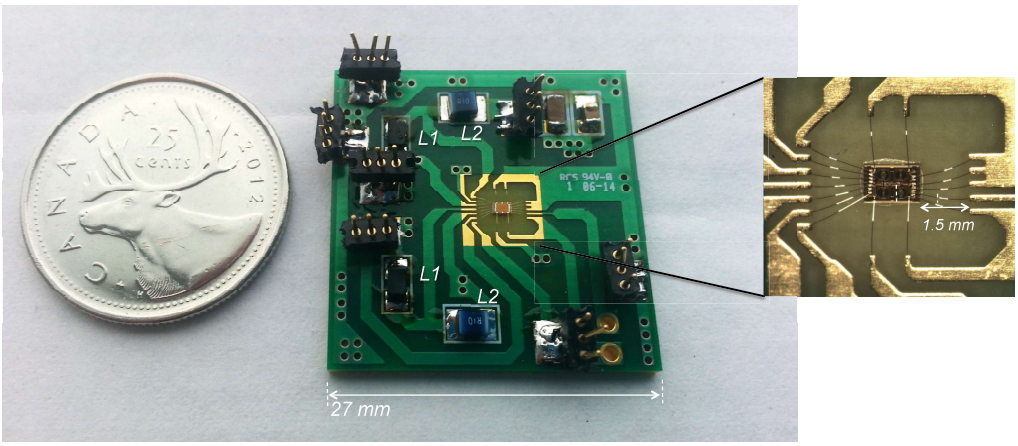

Figure 7: Photograph of the wire-bonded prototype implemented to test the step-up converter.

3.1. The ULV Enhanced-Swing Ring Oscillator

The design of the enhanced-swing ring oscillator (ESRO) follows the guidelines presented in [13, 22]. In order to design a step-up converter able to start-up with V_{DD} of the order of 20 mV, the oscillator was built with high quality off-the-shelf inductors and native transistors. The inductance values are $L_1 = 220$ nH, $L_2 = 595$ nH, both with Q values of around 60 at 50 MHz, which is the approximate value of the oscillation frequency. The dimensions of inductors L_1 and L_2 are 3.2 mm x 1.6 mm x 1.8 mm and 2.5 mm x 2 mm x 1.6 mm, respectively. The zero-VT transistors are composed of a parallel association of 400 MOSFETs, each of them with an aspect ratio of 5 μm / 0.42 μm.

The minimum supply voltage to start up the converter (I_L=0), simulated for the corners of the technology, is shown in Fig. 8. On comparing the simulations run using the typical parameters (tt) with the experiments, the results match very closely.

3.2. ULV Dickson charge pump

The DCP parameters were determined from equations (3) and (6) for the maximum PCE. Considering the ESRO designed, the load specifications ($V_L = 1$ V and $I_L = 1$ μA) and expression (6), we found that the number of stages N and the normalized load current I_L/I_S that lead to the lowest supply voltage for starting up the oscillator are around 11 and 2.5, respectively. After

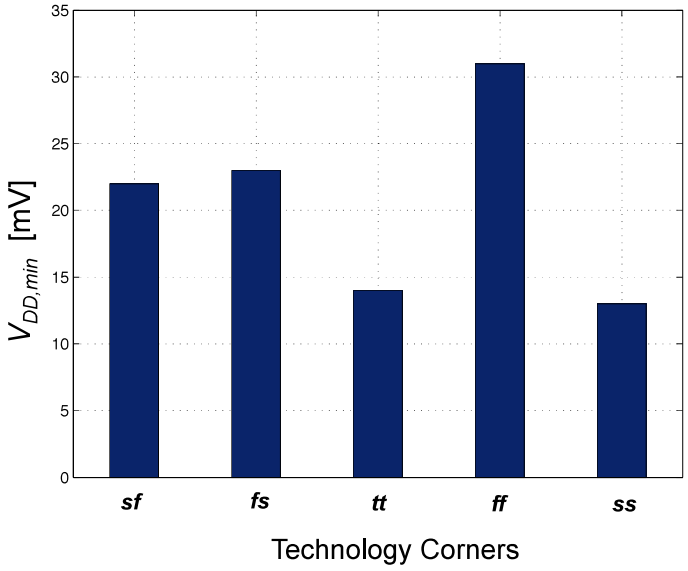

Figure 8: Post-layout simulation of the minimum supply voltage required to start up the converter with $I_L = 0$, for the technology corners.

some tuning through simulation, the requirements for the output voltage and load current were achieved using diode-connected zero-VT transistors in the charge pump, with W/L = 4.2 μm / 0.42 μm, which corresponds roughly to I_S = 550 nA. Coupling capacitors of 2 pF were employed based on the analysis of the ripple voltage, similarly to that described in [1, 20].

4. Experimental results and discussion

The prototype was simulated and experimentally characterized. The complementary oscillator outputs (peak-to-peak voltage of around 110 mV and frequency of 50 MHz) as well as the converter output (V_L= 475 mV) for V_{DD} = 21.8 mV are shown in Fig. 9.

The measurements were taken with the output loaded by the oscilloscope probe, for which R = 10 MΩ and C = 3.3 pF. In order to supply the very small voltage at the converter input, we used the high resolution Keithley 2450 source meter, which gives accurate voltage and measures the DC current. The output voltage was measured using a high impedance voltmeter (Agilent 34411A). To emulate the load current, a Keithley 6221 current source was

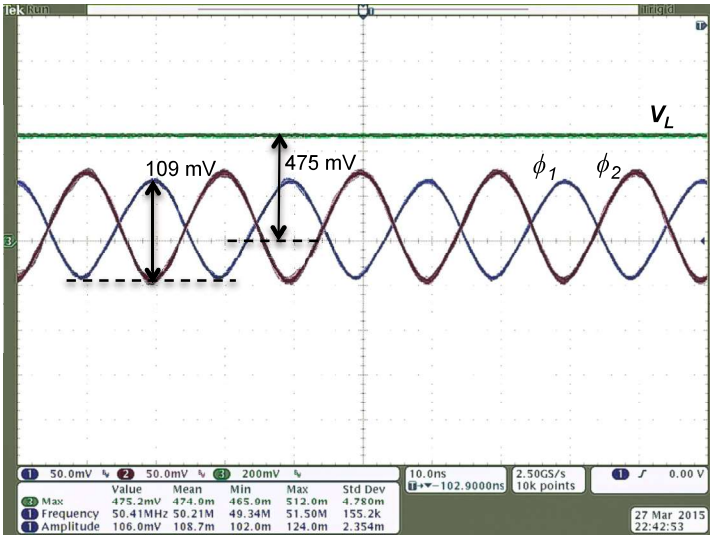

Figure 9: Waveforms of the step-up converter for V_{DD}=21.8 mV and I_L=48 nA. Measurements at the oscillator outputs were taken with 10 MΩ probes.

employed. Figure 10 shows the setup employed to measure the characteristics of the step-up converter.

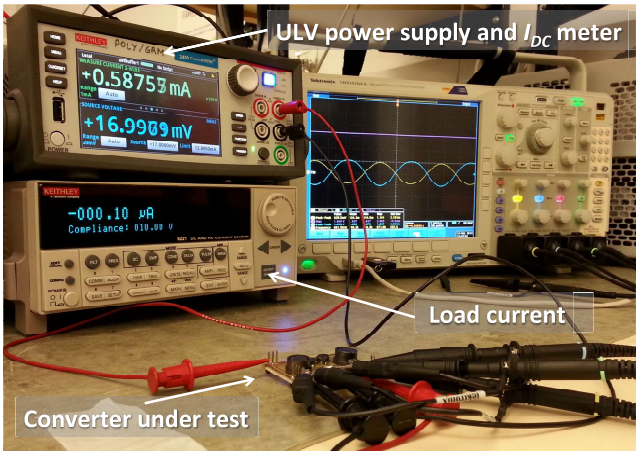

Figure 10: Setup employed to measure the characteristics of the step-up converter.

The transient of the converter is illustrated in Fig. 11, for V_{DD} = 24 mV and I_L = 100 nA. The upper trace is the output voltage of the DCP while the bottom traces are the oscillator outputs.

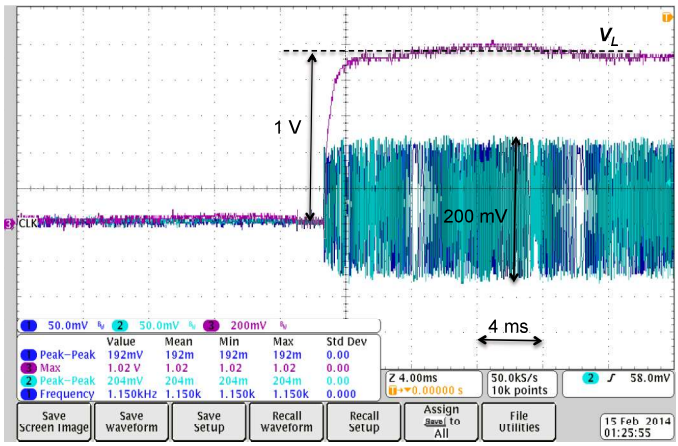

Figure 11: Load voltage V_L and oscillator outputs, loaded with two 10 MΩ probes, of the converter prototype for V_{DD} = 24 mV and I_L = 100 nA.

The output voltage of the DC-DC converter in terms of the input voltage for a 10 MΩ load resistance is shown in Fig. 12. For increasing V_{DD}, the converter starts up at $V_{DD} \approx 17$ mV, giving an output of approximately 750 mV. For decreasing V_{DD}, the converter delivers an output voltage of the order of 400 mV for an input of around 16 mV.

The reason for the difference between the time for the increasing or the decreasing of the supply voltage is that for the increasing V_{DD}, the oscillator has to provide some energy to charge the capacitors in addition to other amounts of energy to compensate the (very small) losses in the diodes. On the other hand, in relation to the decreasing V_{DD}, since the capacitors have already been charged, the amount of energy the oscillator must provide to the charge pump is smaller than that required for the increasing V_{DD}. As the input voltage decreases below 16 mV, the output voltage suddenly vanishes, indicating that the oscillator stops running.

Other experimental results are shown in Fig. 13. The circuit starts up with V_{DD} = 16 mV (at I_L = 10 nA), a value very close to the result of 14 mV obtained from post-layout simulation using typical parameters. The condition I_L = 1 μA and V_L = 1 V is attained at V_{DD} = 23 mV. With V_{DD} = 37.7 mV the converter can supply a load current of 5 μA with V_L = 1 V. The efficiency of the DCP is greatly reduced for low oscillator voltages. As can be seen in Fig. 13 (b), the maximum PCE is around 10 % for an output voltage of 1 V. Also, there is an optimum I_L/I_S ratio that maximizes

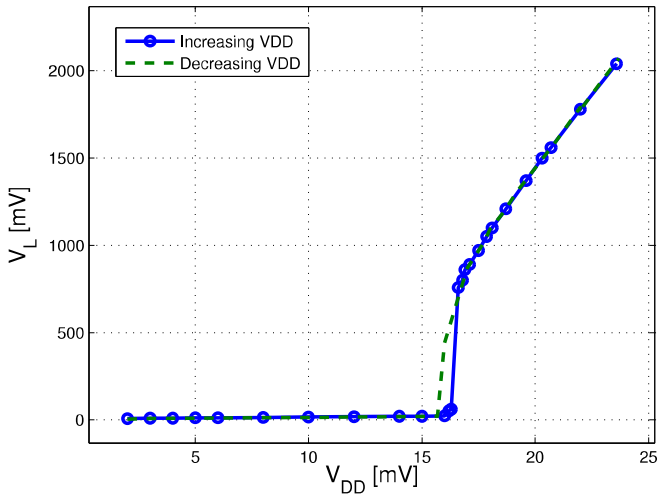

Figure 12: Output voltage of the boost converter associated with increasing and decreasing input voltage. The load resistance is 10 MΩ.

the converter efficiency. For the converter under test, the peak of the overall efficiency is achieved for $I_L = 4$ μA, corresponding to $I_L/I_S = 7.3$ ($I_S = 550$ nA).

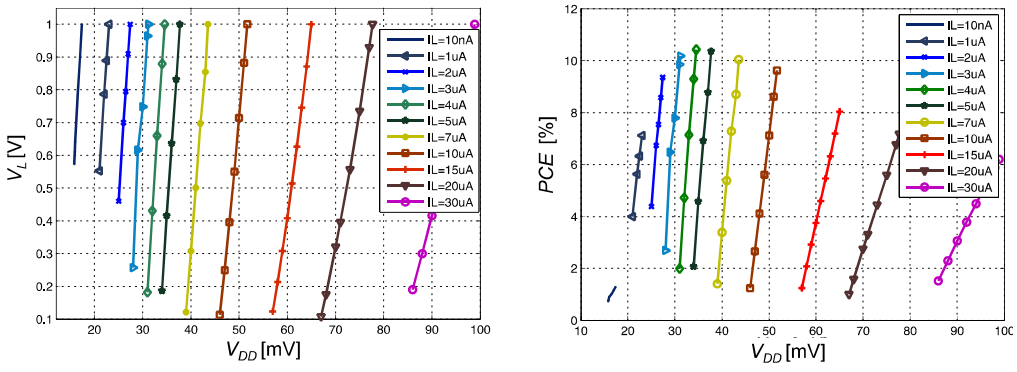

Figure 13: Experimental results for the step-up converter: (a) DC output voltage and (b) power converter efficiency, in terms of the supply voltage (V_{DD}). The maximum measured output voltage was limited to 1 V.

In addition to the measurements, the start-up converter was simulated

for different temperatures. Figure 14 shows that, for a load resistance equal to 100 MΩ, the converter reaches 1 V, for $V_{DD} \approx 20$ mV, in the temperature range from -20 to 20 °C, and to approximately 21.5 mV when the temperature equals 60 °C. The start-up voltage here means that the output voltage of the charge pump is 100 mV, at least. Fig. 14 shows that the converter start-up is strongly influenced by the temperature, as expected [22].

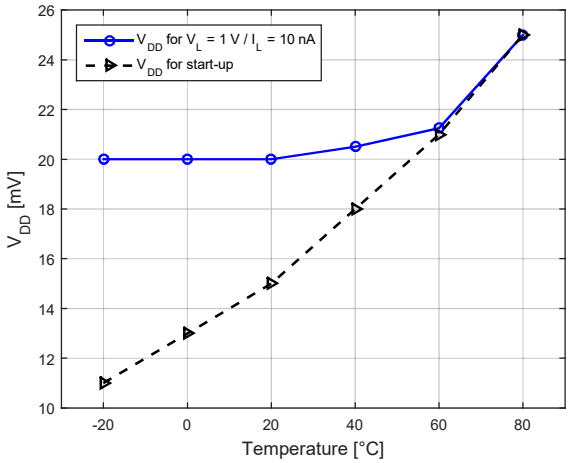

Figure 14: Simulated results of V_{DD} required for start-up and for nominal output voltage (1 V) with a load resistance of 100 MΩ, in terms of temperature (°C).

5. Conclusions

In summary, we have presented an accurate model of the Dickson charge pump, including output voltage, power conversion efficiency, and input resistance. With explicit dependence on the diode parameters, load current, and number of stages, the model is valid from extremely low voltages. A simple expression derived for the input resistance is of great value because it must be considered in the oscillator design, since it directly affects the oscillator start-up voltage.

A converter prototype composed of an enhanced-swing ring oscillator and a Dickson charge pump built in a 130 nm CMOS technology, able to start up from 16 mV, was designed and tested. The analysis presented in this paper offers potential for the design of energy harvesting circuits operating from extremely low voltages, as low as or even less than the thermal voltage.

Appendix A. Diode forward voltage drop and power losses

The average value of the diode current over a complete cycle of the oscillating signal is equal to the load current I_L [20].

$$I_L = \frac{1}{2\pi}\int_{-\pi}^{\pi} I_D d\theta \tag{A.1}$$

Applying (A.1) for both D_1 and D_2 gives

$$I_L = \frac{1}{2\pi}\int_{-\pi}^{\pi} I_S \left[\exp\left(\frac{V_{DD} - V_{C1} - V_A\cos\theta}{n\phi_t}\right)\right] d\theta \tag{A.2}$$

$$I_L = \frac{1}{2\pi}\int_{-\pi}^{\pi} I_S \left[\exp\left(\frac{V_{C1} - V_{C2} - 2V_A\cos\theta}{n\phi_t}\right)\right] d\theta \tag{A.3}$$

where V_{C1} and V_{C2} are the DC voltages of the leftmost and second capacitors in Fig. 2. The solution of (A.2) and (A.3) results in

$$V_{d1} = V_A - n\phi_t \ln\left[\frac{I_0\left(v_a\right)}{1 + I_L/I_S}\right] \tag{A.4}$$

$$V_{d2} = 2V_A - n\phi_t \ln\left[\frac{I_0\left(2v_a\right)}{1 + I_L/I_S}\right] \tag{A.5}$$

where V_{d1} is the forward voltage drop across diodes D_1 and D_N, V_{d2} is the forward voltage drop across the remaining diodes and $I_0(z) = \frac{1}{\pi}\int_0^{\pi} e^{zcos\theta} d\theta$ is the modified Bessel function of the first kind of order zero.

The average power dissipated in the diodes is

$$P_{d1} = \left(I_S + I_L\right) V_A \frac{I_1\left(v_a\right)}{I_0\left(v_a\right)} - I_L n\phi_t \ln\left[\frac{I_0\left(v_a\right)}{1 + I_L/I_S}\right] \tag{A.6}$$

$$P_{d2} = \left(I_S + I_L\right) 2V_A \frac{I_1\left(2v_a\right)}{I_0\left(2v_a\right)} - I_L n\phi_t \ln\left[\frac{I_0\left(2v_a\right)}{1 + I_L/I_S}\right] \tag{A.7}$$

where P_{d1} is the power dissipation in diodes D_1 and D_N, P_{d2} is the power dissipation in the remaining diodes and $I_1(z) = \frac{1}{\pi}\int_0^{\pi} \cos\theta e^{z\cos\theta} d\theta$ is the modified Bessel function of the first kind of order one.

Acknowledgment

The authors are grateful to CMC Microsystems and MOSIS for providing access to integration and to the Brazilian research agencies CAPES, Finance Code 001, and CNPq, for partially funding this study. The authors thank L. Mouden for assembling the samples used in this study.

References

[1] J. F. Dickson, On-chip high-voltage generation in MNOS integrated circuits using an improved voltage multiplier technique, IEEE Journal of Solid-State Circuits 11 (1976) 374–378. doi:10.1109/JSSC.1976.1050739.

[2] T. Tanzawa, Innovation of switched-capacitor voltage multiplier: Part 3: State of the art of switching circuits and applications of charge pumps, IEEE Solid-State Circuits Magazine 8 (2016) 63–73. doi:10.1109/MSSC.2016.2573998.

[3] Y. Zhang, F. Zhang, Y. Shakhsheer, J. D. Silver, A. Klinefelter, M. Nagaraju, J. Boley, J. Pandey, A. Shrivastava, E. J. Carlson, A. Wood, B. H. Calhoun, B. P. Otis, A batteryless 19 μW MICS/ISM-band energy harvesting body sensor node SoC for ExG applications, IEEE Journal of Solid-State Circuits 48 (2013) 199–213. doi:10.1109/JSSC.2012.2221217.

[4] S. Ethier, M. Sawan, Exponential current pulse generation for efficient very high-impedance multisite stimulation, IEEE Transactions on Biomedical Circuits and Systems 5 (2011) 30–38. doi:10.1109/TBCAS.2010.2073707.

[5] R. Vullers, R. Van Schaijk, I. Doms, C. Van Hoof, R. Mertens, Micropower energy harvesting, Solid-State Electronics 53 (2009) 684–693. doi:10.1016/j.sse.2008.12.011.

[6] D. Rozgić, D. Marković, A miniaturized 0.78-mW/cm^2 autonomous thermoelectric energy-harvesting platform for biomedical sensors, IEEE Transactions on Biomedical Circuits and Systems 11 (2017) 773–783. doi:10.1109/TBCAS.2017.2684818.

[7] Y. Qian, D. Lu, J. He, Z. Hong, An on-chip transformer-based self-startup hybrid SIDITO converter for thermoelectric energy harvesting,

IEEE Transactions on Circuits and Systems II: Express Briefs 65 (2018) 1673–1677. doi:10.1109/TCSII.2017.2773564.

[8] S. Yoon, S. Carreon-Bautista, E. Sanchez-Sinencio, An area efficient thermal energy harvester with reconfigurable capacitor charge pump for IoT applications, IEEE Transactions on Circuits and Systems II: Express Briefs 65 (2018) 1974–1978. doi:10.1109/TCSII.2018.2794299.

[9] B. I. Rapoport, J. T. Kedzierski, R. Sarpeshkar, A glucose fuel cell for implantable brain-machine interfaces, PLoS ONE 7 (2012) e38436. doi:10.1371/journal.pone.0038436.

[10] P.-S. Weng, H.-Y. Tang, P.-C. Ku, L.-H. Lu, 50 mV-input batteryless boost converter for thermal energy harvesting, IEEE Journal of Solid-State Circuits 48 (2013) 1031–1041. doi:10.1109/JSSC.2013.2237998.

[11] Y. K. Ramadass, A. P. Chandrakasan, A battery-less thermoelectric energy harvesting interface circuit with 35 mV startup voltage, IEEE Journal of Solid-State Circuits 46 (2011) 333–341. doi:10.1109/JSSC.2010.2074090.

[12] P. Chen, X. Zhang, K. Ishida, Y. Okuma, Y. Ryu, M. Takamiya, T. Sakurai, An 80 mV startup dual-mode boost converter by charge-pumped pulse generator and threshold voltage tuned oscillator with hot carrier injection, IEEE Journal of Solid-State Circuits 47 (2012) 2554–2562. doi:10.1109/JSSC.2012.2210953.

[13] M. B. Machado, M. C. Schneider, M. Sawan, C. Galup-Montoro, Fully-integrated 86 mV - 1 V step-up converter for energy harvesting applications, in: 2014 IEEE 12th International New Circuits and Systems Conference (NEWCAS), 2014, pp. 452–455. doi:10.1109/NEWCAS.2014.6934080.

[14] H. Fuketa, S. O'uchi, T. Matsukawa, Fully integrated, 100-mV minimum input voltage converter with gate-boosted charge pump kick-started by LC oscillator for energy harvesting, IEEE Transactions on Circuits and Systems II: Express Briefs 64 (2017) 392–396. doi:10.1109/TCSII.2016.2573382.

[15] H. M. Jayaweera, A. Muhtaroğlu, Design optimization of a fully integrated charge-pump with LC tank oscillator for ultra-low voltage energy harvesting, Microelectronics Journal 59 (2017) 33–39. doi:10.1016/j.mejo.2016.10.010.

[16] Z. Luo, L. Zeng, B. Lau, Y. Lian, C. Heng, A sub-10 mV power converter with fully integrated self-start, MPPT, and ZCS control for thermoelectric energy harvesting, IEEE Transactions on Circuits and Systems I: Regular Papers 65 (2018) 1744–1757. doi:10.1109/TCSI.2017.2757505.

[17] M. Dezyani, H. Ghafoorifard, S. Sheikhaei, W. A. Serdijn, A 60 mV input voltage, process tolerant start-up system for thermoelectric energy harvesting, IEEE Transactions on Circuits and Systems I: Regular Papers 65 (2018) 3568–3577. doi:10.1109/TCSI.2018.2834312.

[18] B. Lim, J. Seo, S. Lee, A Colpitts oscillator-based self-starting boost converter for thermoelectric energy harvesting with 40-mV startup voltage and 75% maximum efficiency, IEEE Journal of Solid-State Circuits 53 (2018) 3293–3302. doi:10.1109/JSSC.2018.2863951.

[19] K. R. Sadagopan, J. Kang, Y. Ramadass, A. Natarajan, A cm-scale 2.4-GHz wireless energy harvester with nanoWatt boost converter and antenna-rectifier resonance for WiFi powering of sensor nodes, IEEE Journal of Solid-State Circuits 53 (2018) 3396–3406. doi:10.1109/JSSC.2018.2875465.

[20] A. J. Cardoso, L. G. de Carli, C. Galup-Montoro, M. C. Schneider, Analysis of the rectifier circuit valid down to its low-voltage limit, IEEE Transactions on Circuits and Systems I: Regular Papers 59 (2012) 106–112. doi:10.1109/TCSI.2011.2161366.

[21] M. Abramowitz, I. A. Stegun, Handbook of Mathematical Functions with Formulas, Graphs, and Mathematical Tables, Dover Publications, Inc, 1964.

[22] M. B. Machado, M. C. Schneider, C. Galup-Montoro, On the minimum supply voltage for MOSFET oscillators, IEEE Transactions on Circuits and Systems I: Regular Papers 61 (2014) 347–357. doi:10.1109/TCSI.2013.2278344.